doi:10.1016/j.jmb.2006.07.091 J. Mol. Biol. (2006) 362, 1025–1042

JMB

Available online at www.sciencedirect.com

ScienceDirect

ELSEVIER

Assembly of the Archaeal Box C/D sRNP Can Occur *via* Alternative Pathways and Requires Temperature-facilitated sRNA Remodeling

Keith T. Gagnon, Xinxin Zhang, Paul F. Agris and E. Stuart Maxwell*

Department of Molecular and Structural Biochemistry, North Carolina State University Raleigh, NC 27695-7622, USA

*Corresponding author

Archaeal dual-guide box C/D small nucleolar RNA-like RNAs (sRNAs) bind three core proteins in sequential order at both terminal box C/D and internal C′/D′ motifs to assemble two ribonuclear protein (RNP) complexes active in guiding nucleotide methylation. Experiments have investigated the process of box C/D sRNP assembly and the resultant changes in sRNA structure or "remodeling" as a consequence of sRNP core protein binding. Hierarchical assembly of the *Methanocaldococcus jannaschii* sR8 box C/D sRNP is a temperature-dependent process with binding of L7 and Nop56/58 core proteins to the sRNA requiring elevated temperature to facilitate necessary RNA structural dynamics. Circular dichroism (CD) spectroscopy and RNA thermal denaturation revealed an increased order and stability of sRNA folded structure as a result of L7 binding. Subsequent binding of the Nop56/58 and fibrillarin core proteins to the L7–sRNA complex further remodeled sRNA structure. Assessment of sR8 guide region accessibility using complementary RNA oligonucleotide probes revealed significant changes in guide region structure during sRNP assembly. A second dual-guide box C/D sRNA from *M. jannaschii*, sR6, also exhibited RNA remodeling during temperature-dependent sRNP assembly, although core protein binding was affected by sR6's distinct folded structure. Interestingly, the sR6 sRNP followed an alternative assembly pathway, with both guide regions being continuously exposed during sRNP assembly. Further experiments using sR8 mutants possessing alternative guide regions demonstrated that sRNA folded structure induced by specific guide sequences impacted the sRNP assembly pathway. Nevertheless, assembled sRNPs were active for sRNA-guided methylation independent of the pathway followed. Thus, RNA remodeling appears to be a common and requisite feature of archaeal dual-guide box C/D sRNP assembly and formation of the mature sRNP can follow different assembly pathways in generating catalytically active complexes.

Keywords: archaeal sRNA; box C/D RNA; RNA-guided nucleotide methylation; RNA remodeling; RNP assembly

Introduction

Ribonucleotide 2′-*O*-methylation of both eukaryotic and archaeal RNAs is accomplished using box C/D guide RNAs.[1–8] Box C/D RNAs are small species of approximately 50 to 150 nucleotides defined by highly conserved boxes C and D. These terminally located box C and D sequences of six and four nucleotides, respectively, define all box C/D RNAs and are essential for folding the box C/D core motif into characteristic kink-turn, or K-turn, structures.[5,9–12] The K-turn is a helix-asymmetric bulge-helix RNA motif where two G·A base-pairs hydrogen bond across the asymmetric bulge to stabilize the characteristic kinked structure of this RNA motif. Box C/D RNAs often possess internally

Abbreviations used: snoRNA, small nucleolar RNA; sRNA, box C/D snoRNA-like RNAs; sRNP, small ribonuclear protein; K-turn, kink-turn; EMSA, electrophoretic mobility-shift analysis.

E-mail address of the corresponding author: stu_maxwell@ncsu.edu

positioned and highly conserved C′ and D′ boxes that are particularly evident in archaeal box C/D RNAs.[10,13–15] The C′/D′ motif also folds into a K-turn structure. Nucleotide methylation is carried out by base-pairing of guide sequences located upstream of box D and D′ to complementary regions of the target RNA.[1,2,5,16] Core proteins bound to the box C/D and C′/D′ motifs then catalyze 2′-*O*-methylation of the fifth base-paired nucleotide positioned upstream from either box D or D′ (N+5 rule).[1,17–20]

In eukaryotes, four core proteins bind the box C/D small nucleolar RNAs (snoRNAs) and are critical for methylation activity. The 15.5 kDa core protein initiates snoRNP assembly by recognizing the terminal box C/D core motif and stabilizing this RNA element into a K-turn structure.[12,21] Two highly related nucleolar proteins, Nop58 and Nop56, differentially bind the box C/D and C′/D′ motifs, respectively, while the methyltransferase enzyme fibrillarin interacts with both motifs.[22–26] The eukaryotic snoRNP is said to be asymmetric with 15.5 kDa, Nop58, and fibrillarin binding to the terminal box C/D motif and core proteins Nop56 and fibrillarin binding the internal C′/D′ motif.[26,27]

Box C/D snoRNA-like RNAs, or sRNAs, are abundant in archaeal organisms and guide nucleotide methylation of rRNAs and tRNAs.[14,28] *In vitro* assembly of catalytically active archaeal box C/D sRNPs has recently been accomplished and used to structurally and functionally characterize sRNP complexes.[29–33] Archaeal box C/D sRNAs possess characteristic terminal box C/D and internal C′/D′ motifs, each bound by three core proteins which are highly homologous to the eukaryotic box C/D snoRNP core proteins. Ribosomal protein L7, a eukaryotic 15.5 kDa homolog, initiates sRNP assembly by binding both box C/D and C′/D′ motifs.[21,29,30,34] Subsequently, a single homolog for eukaryotic Nop56 and Nop58, Nop56/58 (Nop5), binds both motifs and is followed by fibrillarin binding.[29,30] The three archaeal core proteins exhibit a sequential binding order at both terminal C/D and internal C′/D′ K-turns to establish "symmetric" RNPs of identical protein composition. Optimal methylation activity requires that both box C/D and C′/D′ RNPs be juxtaposed and spatially positioned within the same sRNP complex.[30,31,35] Incomplete assembly caused by mutation, loss of protein components at either the C/D or C′/D′ motif, or alterations in inter-RNP spacing, results in lost or reduced methylation activity from both RNPs. Unfortunately, a complete understanding of box C/D RNP assembly is presently lacking and the nature of inter-RNP interactions is still undefined.[15,36]

Mounting evidence demonstrating that the L7 core protein strongly stabilizes the box C/D K-turn by inducing RNA structural changes has suggested that sRNP assembly requires sRNA remodeling.[37–41] Crystal structures of both free and RNA-bound L7 from several archaeal organisms, as well as FRET analyses, have revealed a mechanism of induced-fit interaction for the RNA component with only minor changes in L7 protein structure upon RNA binding. To further examine this RNA remodeling phenomenon, we have investigated RNA and RNP structural changes induced during assembly of functional archaeal dual-guide box C/D sRNPs. sRNP assembly and concurrent sRNA structural changes were found to be temperature-dependent, indicating that RNA flexibility and remodeling of RNA folded structure are critical for efficient and ordered sRNP assembly. Observed alterations in guide region structure and accessibility during sRNP assembly further reflected RNA remodeling events. Comparison of box C/D sRNAs with different guide regions demonstrated that RNA remodeling can follow alternative pathways during assembly of functional sRNPs. These observations provide another example of RNA remodeling upon protein binding, which is likely a central theme in the assembly of most, if not all, RNP complexes.

Results

Efficient L7 core protein binding is temperature-dependent and requires sRNA remodeling

Box C/D sRNA structural changes induced by core protein binding during sRNP assembly were investigated using our established *in vitro* sRNP assembly system.[30] Recombinant *Methanocaldococcus jannaschii* core proteins L7, Nop56/58, and fibrillarin bind *M. jannaschii* sR8 sRNA *in vitro* to assemble a dual-guide box C/D sRNP complex that is catalytically active in guiding nucleotide 2′-*O*-methylation from both terminal box C/D core and internal C′/D′ RNPs. Elevated temperatures of approximately 70 °C are required for efficient box C/D sRNP assembly and RNA-guided nucleotide modification, consistent with *M. jannaschii* being a thermophilic organism. *M. jannaschii* box C/D sRNA sR8 (Figure 1(a)) was chosen as a model dual-guide box C/D sRNA, having perfect consensus C, C′, D, and D′ boxes with D and D′ guide regions of 12 nucleotides each. Box C/D and C′/D′ motifs fold into K-turn elements and their inter-motif spacing of 12 nucleotides is highly conserved in Archaea.[13,35]

L7 initiates sRNP assembly at both box C/D core and C′/D′ motifs with an L7 core protein binding each motif in a cooperative manner.[30] Titration of L7 with radiolabeled sR8 at the optimal binding temperature of 70 °C revealed the formation of two RNP complexes as L7 concentration increased, consistent with L7 binding to one and then the second RNA motif (Figure 1(b)). Strikingly, elevated temperature was required for simultaneous L7 binding to both RNA motifs. At low temperature of 4 °C, only a single L7 protein was bound (Figure 1(b)). This phenomenon was dependent

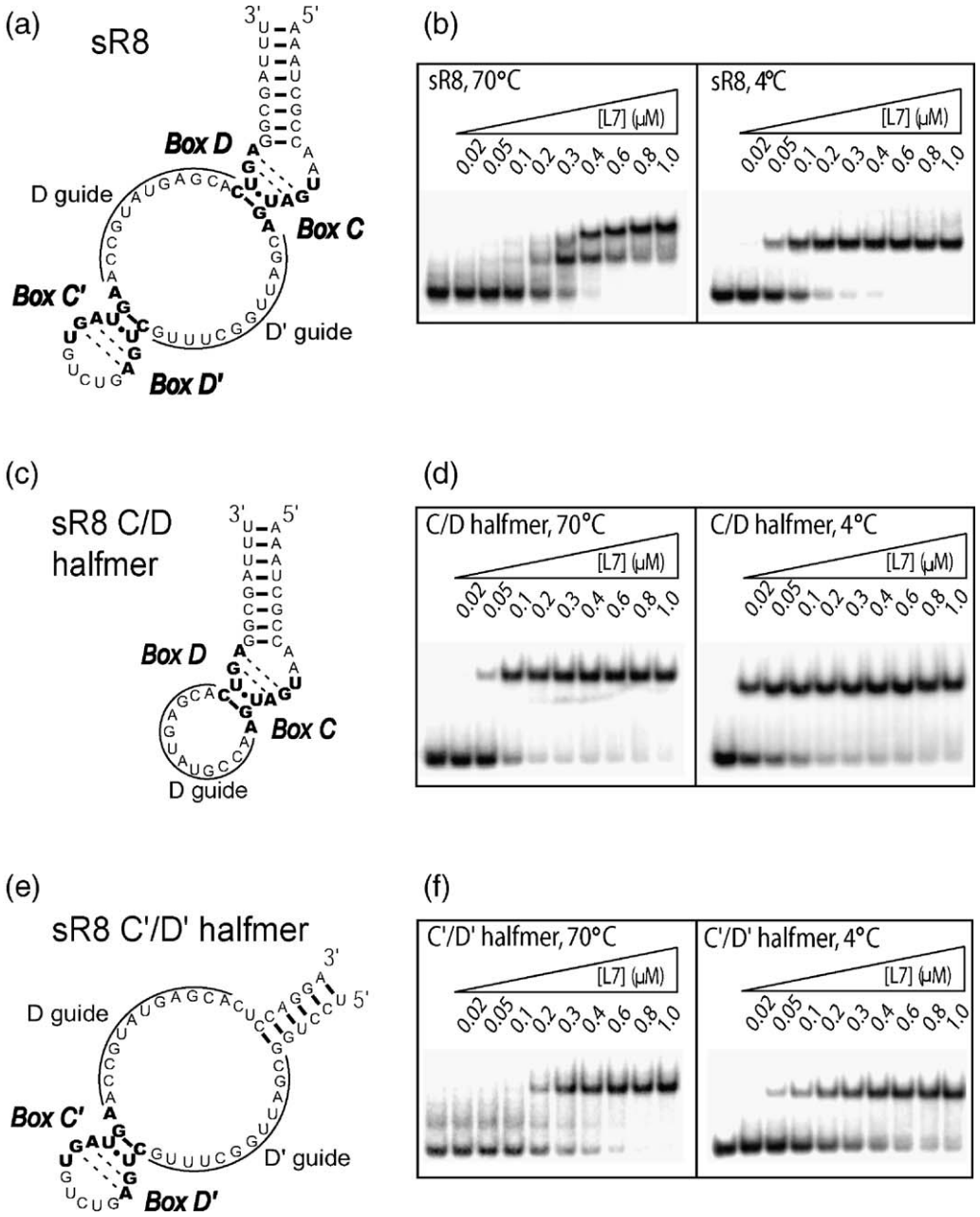

Figure 1. L7 core protein binding to both sR8 box C/D and C′/D′ motifs requires elevated assembly temperatures. (a) Folded secondary structure of *M. jannaschii* sR8 box C/D sRNA. Conserved boxes C/D and C′/D′ sequences are in bold. D and D′ guide regions are indicated. (b) Electrophoretic mobility-shift analysis (EMSA) of L7 binding to sR8 sRNA at low and elevated temperatures. Radiolabeled sR8 was incubated with increasing concentrations of L7 at 70 °C (left) or 4 °C (right) and resultant RNPs resolved on native polyacrylamide gels at 4 °C. (c) and (e) Folded secondary structures of sR8 half-mer RNAs possessing box C/D and C′/D′ motifs. (d) and (f) EMSA analysis of L7 binding to box C/D and C′/D′ half-mer RNAs at low and elevated temperatures. Radiolabeled sR8 half-mer RNAs were incubated with increasing concentrations of L7 at 70 °C or 4 °C and the resultant RNPs resolved on native polyacrylamide gels at 4 °C.

upon having both RNA motifs contained in a single RNA molecule. sR8 "half-mer" RNAs possessing only box C/D or C′/D′ motifs (Figure 1(c) and (e)) bound a single L7 protein at both low and elevated temperatures (Figure 1(d) and (f)). Since the L7 protein does not undergo significant structural changes during K-turn binding,[40] we concluded that elevated temperature was necessary to enhance the flexibility and conformational freedom of the sRNA, thus facilitating L7 binding through RNA "remodeling" of both motifs juxtaposed in the same sRNA molecule.

L7 binding remodels and stabilizes sR8 sRNA structure

The effect of L7 core protein binding upon sR8 sRNA structure was assessed using circular

dichroism (CD) spectroscopy, thermal denaturation analysis, and nuclease mapping. CD analysis revealed that L7 binding at low temperature (4 °C) increased the amplitude of the positive ellipticity at 260 nm ($\Delta\varepsilon_{260}$), indicating a more ordered or structured sRNA (Figure 2(a)). Protein spectra at this wavelength was negligible and this baseline was subtracted so as not to interfere with data interpretation. Thus, increased ellipticity reflected enhanced sRNA base–base interactions and base stacking. This increase in ordered structure was further enhanced when L7 binding was carried out at elevated temperature (70 °C) where L7 is bound to both the box C/D and C′/D′ motifs. The two different CD curves obtained at different assembly temperatures suggest that different sRNA structures exist when sR8 is bound at 4 °C or 70 °C with one or two L7 molecules, respectively. No difference in CD spectra was observed at these two temperatures for sRNA alone, clearly demonstrating that the observed increase was dependent upon L7 binding.

Thermal denaturation analysis of the sR8 sRNA in the presence of increasing amounts of L7 protein revealed a stabilization of RNA structure upon protein binding (Figure 2(b)). An increase in

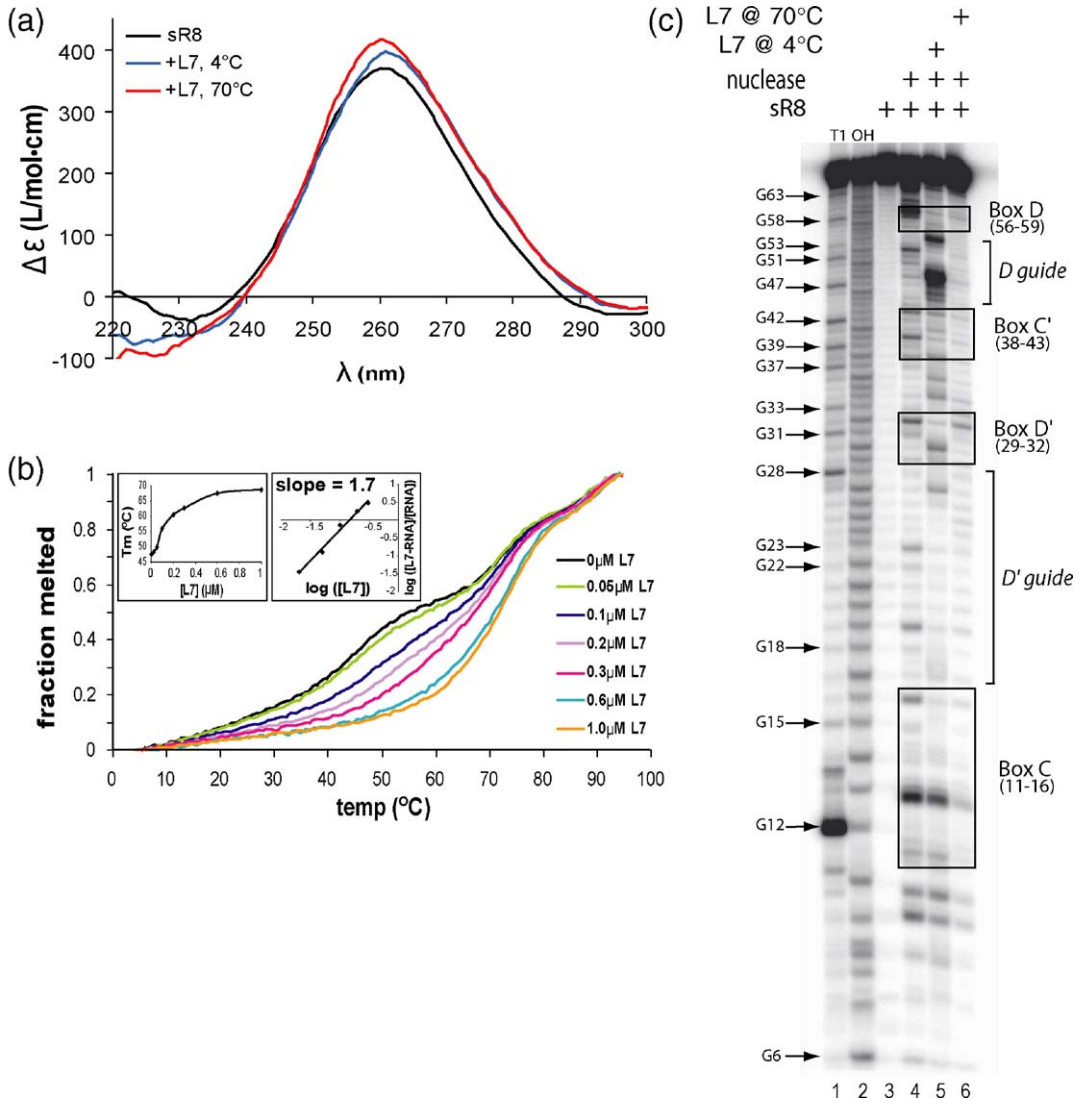

Figure 2. L7 binding to sR8 remodels and stabilizes sRNA structure. (a) CD spectroscopy of L7 core protein binding to sR8 sRNA at low and elevated RNP assembly temperatures. Protein-only baselines were subtracted. (b) Thermal denaturation analysis of L7 binding to sR8 sRNA at increasing concentrations of L7 core protein. Insets are a plot of T_m as a function of L7 concentration and a Hill plot calculation of the data. Protein-only baselines were subtracted. (c) Mung bean nuclease mapping of L7–sR8 RNP complexes assembled at low and elevated temperatures. Radiolabeled sR8 was bound with L7 at low (4 °C) and elevated (70 °C) temperature, probed with mung bean nuclease at 4 °C, and resulting RNA fragments resolved on a denaturing polyacrylamide sequencing gel. Reaction components and assembly temperatures are indicated above each lane. Nucleotide sequencing ladders were generated by RNase T1 digestion (T1) and alkaline hydrolysis (OH). Box C, D, C′, and D′ sequences are enclosed and D and D′ guide regions designated by brackets.

T_m of 17.3(±0.4) °C was observed, with a corresponding decrease in free energy calculated at 4.5(±0.6) kcal/mol (Meltwin 3.5), when sR8 was bound by two L7 molecules. Plotting the change in T_m as a function of L7 concentration yielded a sigmoidal curve, which, when plotted using the Hill equation, gave a Hill coefficient of 1.7, indicating strong cooperativity (Figure 2(c), inset). This is consistent with previous observations.[30] These results indicate that sR8 conformational changes contribute to the observed cooperativity of L7 core protein binding.

To further investigate sRNA remodeling induced by L7 binding, nuclease mapping with a single strand-sensitive nuclease, mung bean nuclease, was performed at 4 °C after binding L7 at either 4 °C or 70 °C. The low nuclease digestion temperature was necessary to ensure that the RNP assembled at low temperature bound only one L7 protein. Limited digestion of unbound 5′-radiolabeled sR8 at 4 °C yielded a pattern of nuclease cleavage sites throughout the sRNA (Figure 2(c), lane 4). Binding of L7 at 4 °C significantly altered this digestion pattern in boxes D, D′ and C′ (lane 5). Reduction in nuclease cleavage could be due to protection by protein binding or induced RNA structural changes. However, enhancement of cleavage, such as observed in the D guide region and in box D′ (U30), clearly demonstrated induced RNA structural changes. Unfortunately, these results did not clearly indicate whether L7 was uniquely binding the box C/D or C′/D′ motif. This may suggest that either motif can be bound at this temperature but not both. Nuclease mapping of L7 titration onto sR8 at elevated temperature has also been inconclusive in determining an order of L7 binding (data not shown). Comparison of nuclease digestion when L7 was bound at 4 °C *versus* 70 °C revealed unique cleavage sites for each L7 binding temperature. Most distinct was a large reduction in cleavage of the D guide region when L7 was bound at 70 °C (lane 6). Thus, the final sR8 folded structure is dependent upon L7 binding temperature and full occupancy of both RNA motifs.

Ordered assembly of the sR8 sRNP is temperature-dependent and requires sRNA structural changes

Assembly of box C/D sRNPs was characterized by sequential binding of the core proteins, with L7 binding followed by Nop56/58 and fibrillarin binding. Analysis of the sR8 assembly pathway revealed that, as with L7, binding of Nop56/58 was also a temperature-dependent process that required changes in sR8 sRNA structure and/or dynamics. As shown previously, L7 binding to both motifs to initiate sRNP assembly required elevated temperature (Figure 3(a), lane 2 *versus* lane 6). When only one L7 was bound to sR8 (low temperature), neither Nop56/58 nor fibrillarin were able to bind (Figure 3(a), lanes 3 and 4). Notably, when L7 was bound to box C/D and C′/D′ motifs, Nop56/58 still required elevated temperature for binding (Figure 3(a), lanes 7 *versus* lane 11). Prior Nop56/58 dimerization with fibrillarin also did not affect Nop56/58's requirement for elevated temperature to bind (data not shown). These results indicated that Nop56/58 binding also required RNA conformational flexibility or structural remodeling. Prior heating of Nop56/58 did not facilitate its binding, implying that necessary structural changes promoted by elevated temperature occur in the sRNA and not the protein (data not shown). Once Nop56/58 was bound, fibrillarin was able to bind independent of temperature (Figure 3(a), lanes 12 and 16). This is consistent with previous work demonstrating that Nop56/58 and fibrillarin dimerize in the absence of sRNA, suggesting that fibrillarin binding occurs primarily through protein–protein contacts.[29,30,42]

To assess alterations in sRNA structure during full sRNP assembly, both CD and thermal denaturation experiments were carried out. In these experiments, Nop56/58 tended to precipitate at elevated temperature unless complexed with fibrillarin. Therefore, an assessment of their individual contributions for altering sRNA structure was not possible. CD experiments revealed a pronounced increase in peak amplitude at 260 nm ($\Delta\varepsilon_{260}$) upon Nop56/58-fibrillarin binding, most likely reflecting increased order and base stacking of individual sR8 nucleotides in an already well folded sRNA (Figure 3(b)).[43–45] Analysis of sR8's thermal melting profile revealed that after strong stabilization of sR8 structure by L7 binding, only slight alterations in the profile were observed with Nop56/58-fibrillarin binding (Figure 3(c)). From these experiments, we concluded that the initial binding of L7 dramatically stabilizes sRNA structure while subsequent binding of the Nop56/58-fibrillarin dimer primarily affects nucleotide order and base stacking.

sRNA and sRNP structure were also investigated during full sRNP (70 °C) assembly with nuclease mapping (Figure 3(d)). The conserved G and A nucleotides of boxes C (G12, A13) and D (G58, A59), as well as the protruded uridine and adjacent adenine of box C (U11, A10), displayed a cleavage pattern consistent with their exposed locations in the asymmetric bulge region of the box C/D core motif.[41,46] Cleavage sites were also observed in boxes C′ and D′ as well as the D guide region (Figure 3(d), lane 3). Consistent with previous observations, binding of L7 to sR8 resulted in the protection of boxes C, D, and C′, enhancement of box D′ cleavage, and small changes in the D guide region (Figure 3(d), lane 4). Subsequent binding of Nop56/58 protected box D′, slightly altered D guide region structure, and increased protection at boxes C′ and C (lane 5). Final binding of fibrillarin generated only minor changes in the digestion pattern (lane 6). Similar box C/D RNA structural changes have also been reported during assembly of a box C/D RNA

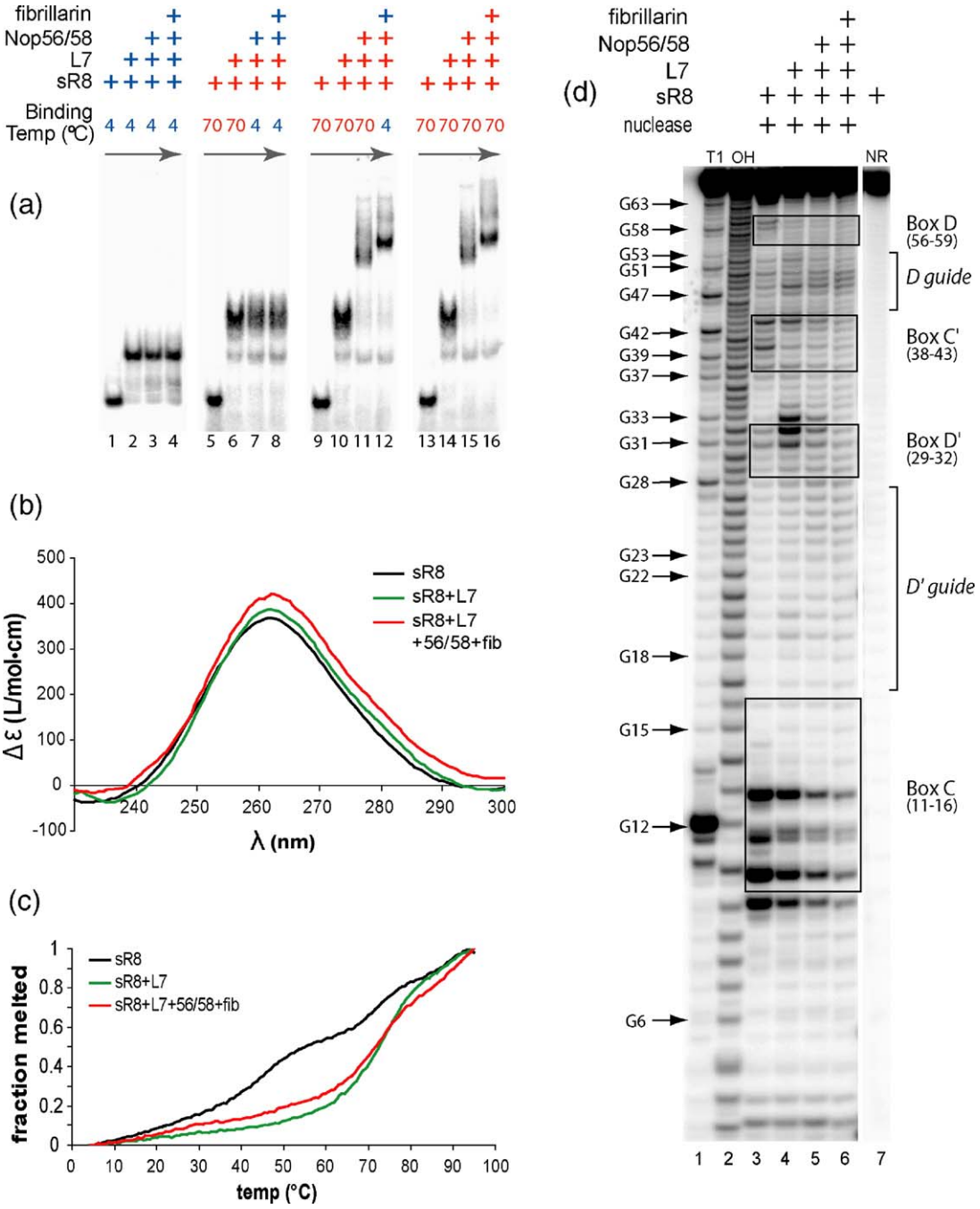

Figure 3. Complete assembly of the sR8 sRNP complex requires elevated assembly temperatures and sRNA remodeling. (a) Assembly of the sR8 sRNP complex by sequential addition of core proteins at low and elevated assembly temperatures. Radiolabeled sR8 was incubated sequentially with L7, Nop56/58, and fibrillarin core proteins at 4 °C or 70 °C and resulting RNP complexes resolved on native polyacrylamide gels at 4 °C. Indicated above each gel lane are the components for each assembly step with the respective incubation temperature. Arrows indicate the order of protein addition for individual assembly reactions. (b) CD spectroscopy of sR8 sRNP assembly. (c) Thermal denaturation analysis of sR8 sRNP assembly. (d) Mung bean nuclease mapping of sR8 sRNP assembly. 5′-Radiolabeled sR8 was sequentially bound with L7, Nop56/58, and fibrillarin core proteins at 70 °C and the assembled RNPs then probed with mung bean nuclease at room temperature. Resulting sRNA fragments were resolved on a denaturing polyacrylamide sequencing gel. Reaction components are indicated above each lane. Nucleotide sequencing ladders were generated by RNase T1 digestion (T1) and alkaline hydrolysis (OH). No reaction (NR) is radiolabeled sR8 not digested with nuclease. Box C, D, C′, and D′ sequences are enclosed by boxes and D and D′ guide sequences designated by brackets.

embedded in the pre-tRNA^{Trp} RNA from *Haloferax volcanii* and *Pyrococcus abyssi* using Pb^{2+}-induced RNA cleavage.[32] These cleavage patterns reflect not only protection from digestion as core proteins bind, but also changes in sRNA structure or remodeling as sRNP assembly proceeds.

sR8 sRNA remodeling modulates D and D′ guide sequence accessibility for target RNA binding

Small changes in sR8 guide sequence structures seen in nuclease mapping experiments prompted us to explore their accessibility for target RNA binding during sRNP assembly. Short RNA oligonucleotides complementary to the sR8 D and D′ guide sequences (target RNA probes) were tested for their ability to base-pair to the guide sequences during sRNP assembly. RNA duplex formation was monitored by Pb^{2+} probing, where the sRNA is preferentially cleaved in flexible and/or single-stranded regions (Figure 4(a)). The utilization of Pb^{2+} as an RNA structural probe produced somewhat different digestion patterns than mung bean nuclease. This is due to the small size of the metal ion and its ability to examine in more detail the fine structure of the folded sRNA and its guide regions. Cleavage results demonstrate that the D, but not D′, guide region was accessible for base-pairing with its complementary RNA probe as evidenced by D guide region protection from Pb^{2+} cleavage when the D target RNA was present (Figure 4(a), lanes 4–7). L7 binding to sR8 induced a characteristic cleavage pattern (both enhanced and protected nucleotides) in both D and D′ guide regions, indicating significant sRNA structural changes. Particularly prominent was a strong cleavage at nucleotide C54 of the D guide region (Figure 4(a), lane 8). Addition of D and D′ target RNA probes did not significantly alter this digestion pattern, indicating that the binding of the L7 core protein inhibited target RNA binding (Figure 4(a), lanes 9–11). Electrophoretic mobility-shift analysis (EMSA) of radiolabeled target RNA binding to sR8 in the absence and presence of L7 at low temperature (4 °C) further suggested that L7 causes structural changes during binding that are not conducive to target RNA binding, since L7 was unable to bind sR8 when the D target RNA was bound first (Figure 4(b)). The converse was also true. Radiolabeled D target RNA incubated with sR8 already bound by L7 was unable to bind its sRNA guide sequence (data not shown). These data indicate that L7 binding to sR8 requires RNA structural dynamics and guide region remodeling. The D′ target did not bind sR8 independent of whether the sRNA was or was not bound with L7, suggesting that the D′ guide sequence is locally folded to prevent target RNA probe base-pairing.

Binding of Nop56/58 and fibrillarin core proteins further altered Pb^{2+} cleavage patterns of the D and D′ guide sequences (Figure 4(a), lane 12). Addition of D and D′ target RNA probes protected the D and D′ guide sequences, respectively, showing that both guide regions were accessible for base-pairing upon full sRNP assembly (Figure 4(a), lanes 13–15). EMSA of radiolabeled target RNA binding to sR8 at each sRNP assembly step has supported the conclusions of these mapping experiments (data not shown). Also, the use of target RNA probes methylated at the target nucleotide showed no difference in target

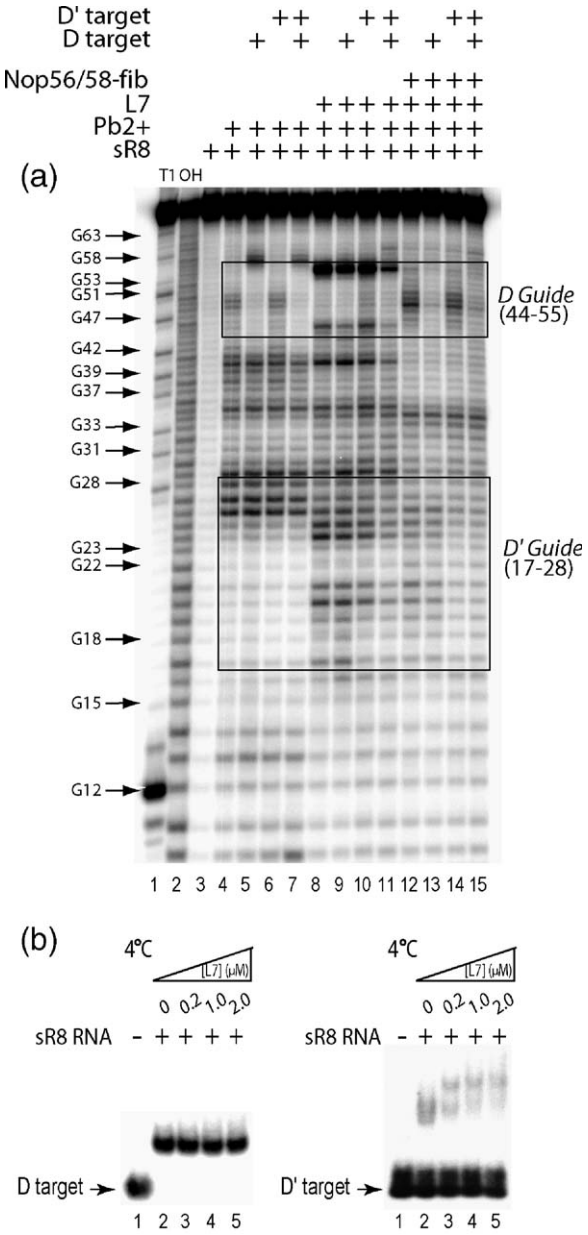

Figure 4. sR8 D and D′ guide region accessibility to target RNA binding changes during sRNP assembly. (a) Assessment of sR8 D and D′ guide region accessibility to target RNA base-pairing using lead (Pb^{2+}) cleavage probing. Radiolabeled sR8 was sequentially assembled with sRNP core proteins, incubated with D and/or D′ target RNAs, and then cleaved with Pb^{2+}. sR8 sRNA cleavage products were resolved on a denaturing polyacrylamide sequencing gel. Components of the individual assembly reactions are indicated above each gel lane. Nucleotide sequencing ladders were generated by RNase T1 digestion (T1) and alkaline hydrolysis (OH). (b) EMSA of target RNA oligonucleotide binding to sR8 D and D′ guide sequences in the presence of L7 core protein. Radiolabeled D (left panel) and D′ (right panel) target RNA probes were incubated with non-radiolabeled sR8 sRNA at 4 °C in the presence of increasing concentrations of L7. Free RNA, RNA–RNA hybrids, and assembled RNPs were resolved on native polyacrylamide gels at 4 °C.

RNA binding (data not shown). Collectively, these analyses demonstrated that the D and D′ guide sequences undergo distinct structural changes during sR8 sRNP assembly. Notably, both guide regions become fully accessible to target RNA binding only upon complete sRNP assembly with all three core proteins.

Temperature-dependent assembly of *M. jannaschii* sR6 sRNP requires sRNA remodeling but uses an alternative assembly pathway

To determine if temperature-dependent sRNP assembly and sRNA remodeling are general features of archaeal box C/D sRNP biosynthesis, a second box C/D sRNA from *M. jannaschii*, sR6, was selected for analysis. sR6 is also a dual-guide sRNA possessing box C/D and C′/D′ motifs separated by inter-motif spacing distances of 12 nucleotides (Figure 5(a)). The distinguishing structural difference between sR6 and sR8 is the D and D′ guide sequences, which are complementary to different target RNAs (Figure 8(a)). Examination of L7 binding to sR6 in titration experiments revealed more efficient binding at an elevated temperature (Figure 5(b)). Interestingly, even at elevated temperature L7 appeared to bind only once. The gradual decrease in RNP mobility suggested that alternative sRNA structures or remodeling may be occurring during L7 binding. A similar effect has been observed for the binding of the 15.5 kDa protein, the eukaryotic homolog of L7, to the human U15 snoRNA.[30] To confirm that L7 was binding only once, an affinity isolation protocol was developed. Both N-terminally His-tagged and untagged L7 were incubated with sR6 at elevated temperature. Assembled RNPs were then affinity selected using the His tag. Low levels of untagged L7 were co-purified with the selected His-L7–sR6 complex (Figure 5(c)). In contrast, similar affinity selection of assembled His-L7–sR8 complexes co-purified much higher amounts of untagged L7 protein. These results indicated only very weak binding of a second L7 to sR6.

Temperature-dependent assembly of the complete sR6 sRNP was examined next (Figure 6(a)). Similar to sR8 sRNP assembly, elevated temperatures were required for efficient Nop56/58 binding. Some Nop56/58 binding was observed at 4 °C, but complete conversion of the L7–sR6 RNP to a larger complex containing Nop56/58 clearly required elevated temperature (Figure 6(a), lane 7 *versus* lane 11). Interestingly, subsequent binding of fibrillarin at either 4 °C or 70 °C did not result in the presence of a prominent, slower migrating (larger) complex (Figure 6(a), lanes 12 and 16). Rather, the appearance of a faster migrating complex, particularly evident at 70 °C, indicated that full complex assembly may result in sRNP compaction. A similar observation has been made for fibrillarin binding in the assembly of the eukaryotic box C/D snoRNP (K. T.G., X.Z. & E.S.M., unpublished results). Assembly

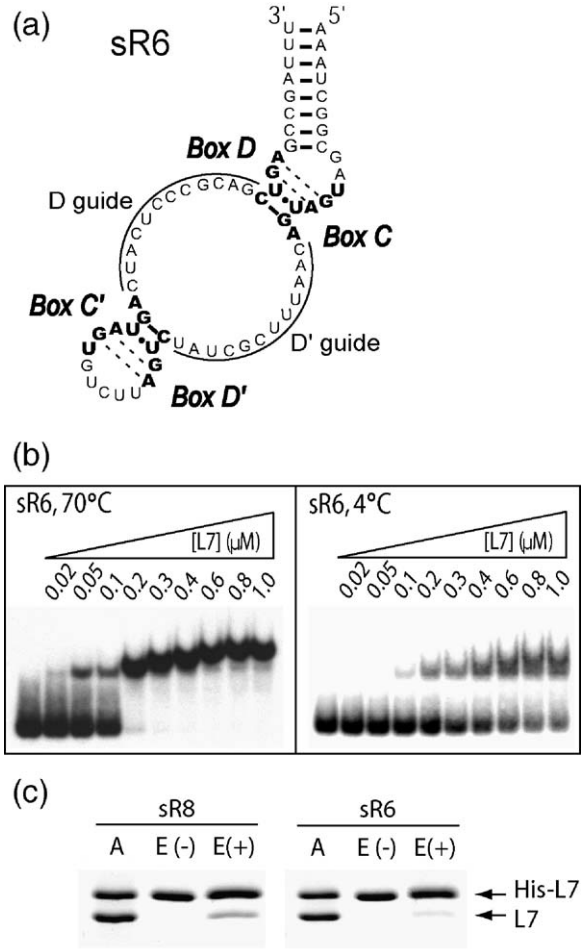

Figure 5. *M. jannaschii* sR6 requires elevated temperature for efficient L7 binding. (a) *M. jannaschii* sR6 folded secondary structure. Box C, D, C′, and D′ sequences are presented in bold with D and D′ guide sequences indicated. (b) Efficient L7 binding to sR6 sRNA requires elevated temperatures. Radiolabeled sR6 sRNA was bound with increasing concentrations of L7 core protein at 70 °C or 4 °C and resultant RNPs resolved on native polyacrylamide gels at 4 °C. Concentrations of added L7 protein are indicated above each gel lane. (c) sR6 efficiently binds only one L7 core protein. His-tagged and non-tagged L7 proteins were incubated with sR8 or sR6 sRNAs at 70 °C and assembled L7–sRNA complexes isolated by nickel affinity chromatography. Isolated proteins were resolved by SDS-PAGE and stained with Coomassie blue. A, proteins incubated with sRNA; E(-), L7 proteins incubated without sRNA and affinity purified; E(+), L7 proteins incubated with sRNA and affinity purified.

of fully functional sR6 sRNP complexes was confirmed in methylation assays (Table 1).

CD and thermal denaturation analyses, along with nuclease mapping of the assembling complex, were used to further investigate sR6 sRNP assembly. As observed with the sR8 sRNP, CD analysis revealed a stepwise ordering of the sR6 sRNA structure upon sequential core protein binding (Figure 6(b)). Thermal denaturation experiments demonstrated an increase in the T_m value (~20.8 °C) upon L7 binding.

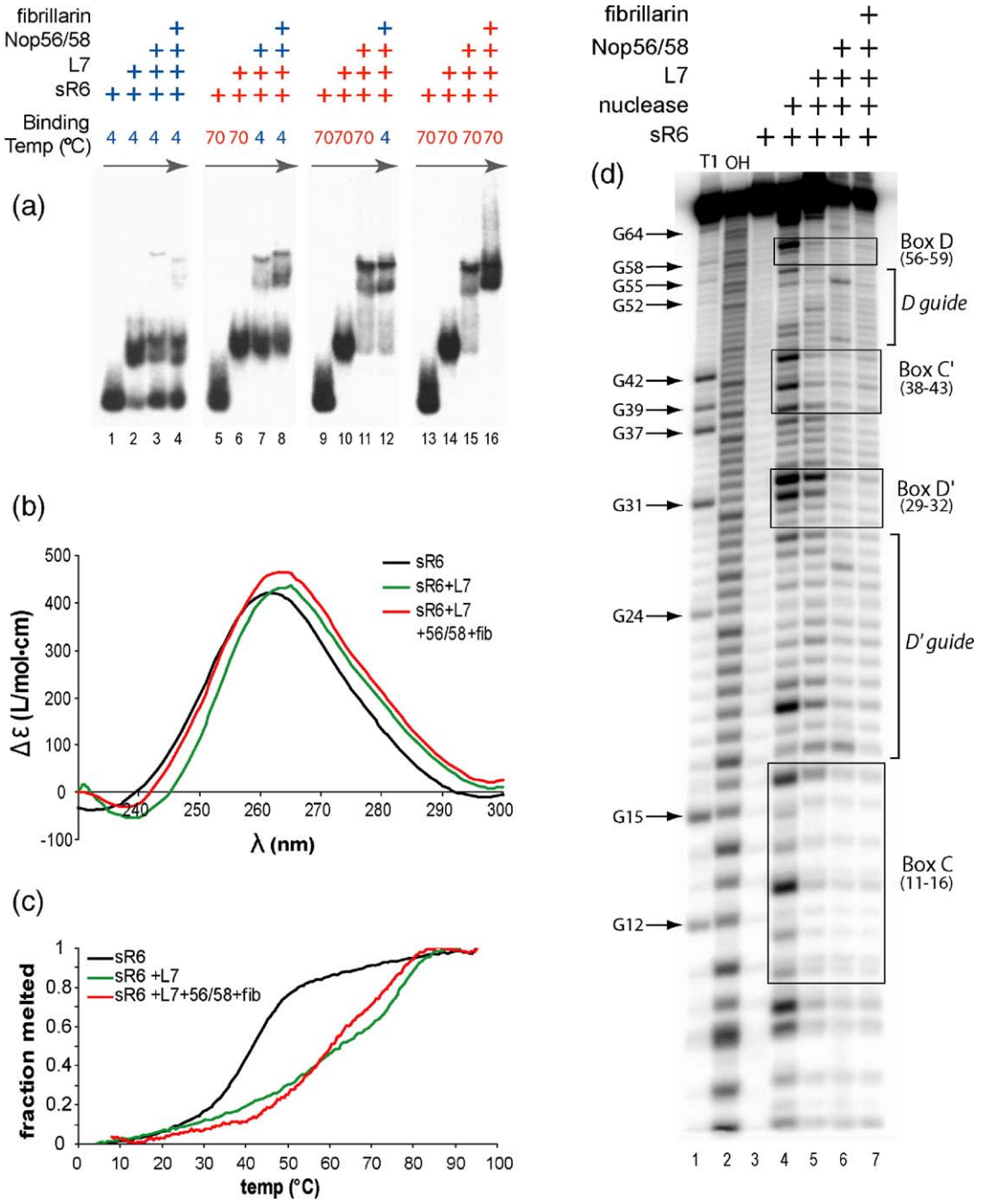

Figure 6. sR6 sRNP assembly requires sRNA remodeling. (a) The sR6 sRNP requires elevated temperature for efficient assembly. Radiolabeled sR6 sRNA was incubated sequentially with L7, Nop56/58, and fibrillarin core proteins at 4 °C or 70 °C and the resulting RNP complexes were resolved on a native polyacrylamide gel at 4 °C. Indicated above each gel lane are the components for each assembly step as well as the respective incubation temperatures. Arrows indicate the order of core protein addition for individual assembly reactions. (b) CD spectroscopy of sR6 sRNP assembly. (c) Thermal denaturation analysis of sR6 during sRNP assembly. (d) Mung bean nuclease mapping of sR6 during sRNP assembly. 5′-Radiolabeled sR6 was sequentially bound with L7, Nop56/58, and fibrillarin core proteins at 70 °C followed by mung bean nuclease probing at room temperature. sRNA fragments were resolved on a denaturing polyacrylamide sequencing gel. Reaction components of each assembly reaction are indicated above each gel lane. Nucleotide sequencing ladders were generated by RNase T1 digestion (T1) and alkaline hydrolysis (OH). Box C, D, C′, and D′ sequences are enclosed by boxes and D and D′ guide sequences designated by brackets.

Binding of the Nop56/58-fibrillarin dimer only slightly altered the melting curve profile (Figure 6(c)). Of particular note, however, was a difference in the melting curve profile of free sR6 sRNA compared with that of free sR8 (Figure 3(c)). Melting of sR8 yielded a biphasic melting curve whereas that of sR6 was monophasic. Since the major difference between these two sRNAs is their respective guide sequences (Figure 8(a), below), we concluded that the difference in melting profiles was due to the

Table 1. 2′-*O*-Methylation activity of dual-guide box C/D sRNPs

Guide RNA	D target pmol/60 min minus D-CH3 background (% of WT sR8)	D′ target pmol/60 min minus D′CH3 background (% of WT sR8)
sR8	12.3±0.2 (100)	12.9±0.3 (100)
sR6	16.2±0.6 (131)	16.5±1.9 (127)
sR8 GRrev	14.9±2.5 (120)	11.0±0.5 (85)
sR8 GRsr6	15.1±0.7 (123)	15.2±0.4 (117)

WT, wild-type.

distinctly folded structures of the guide sequences of each sRNA (see below).

Nuclease mapping experiments assessed changes in sR6 RNA structure during sRNP assembly (Figure 6(d)). Prior to core protein binding, boxes C, D, C′, and D′ are clearly accessible, similar to sR8 sRNA. L7 binding protected boxes C, D, and C′ sequences from cleavage with smaller effects for box D′. Since L7 appeared to bind to both motifs and previous experiments indicated a single L7-bound sR6, we concluded that initial binding of a single L7 protein could be at either motif. Only when Nop56/58 was added did box D′ become significantly protected. As with the sR8 sRNP, the binding of fibrillarin had modest effects on the digestion pattern, consistent with its binding primarily through protein–protein interactions with Nop56/58. Cleavage patterns of the sR6 box C/D and C′/D′ motifs upon core protein binding were very similar to those observed during sR8 sRNP assembly. However, different cleavage patterns were noted in the sR6 and sR8 guide regions, again suggesting distinctly folded structures for the respective sRNA guide sequences.

sR6 guide regions are exposed throughout sRNP assembly

Accessibility of sR6 guide regions for target RNA probe base-pairing during sRNP assembly was assessed by probing with Pb^{2+} (Figure 7(a)). In surprising contrast to sR8, both D and D′ guide regions were available to bind their respective target RNAs throughout sRNP assembly. Both target RNAs bound free sR6 (lanes 4–7) as well as when sR6 was bound with core proteins (lanes 8–15). Consistent with these observations, and in contrast to sR8, L7 binding to sR6 at low temperatures was largely unaffected by bound D and D′ target RNA probes (Figure 7(b)).

sRNA guide sequences can influence the sRNP assembly and remodeling pathway

Analysis of sR6 and sR8 sRNP assembly suggested that the sRNA-specific guide sequences could affect the assembly and remodeling pathway. To investigate further the influence of D and D′ guide sequences upon box C/D sRNP assembly two sR8 sRNA guide region mutants were engineered to

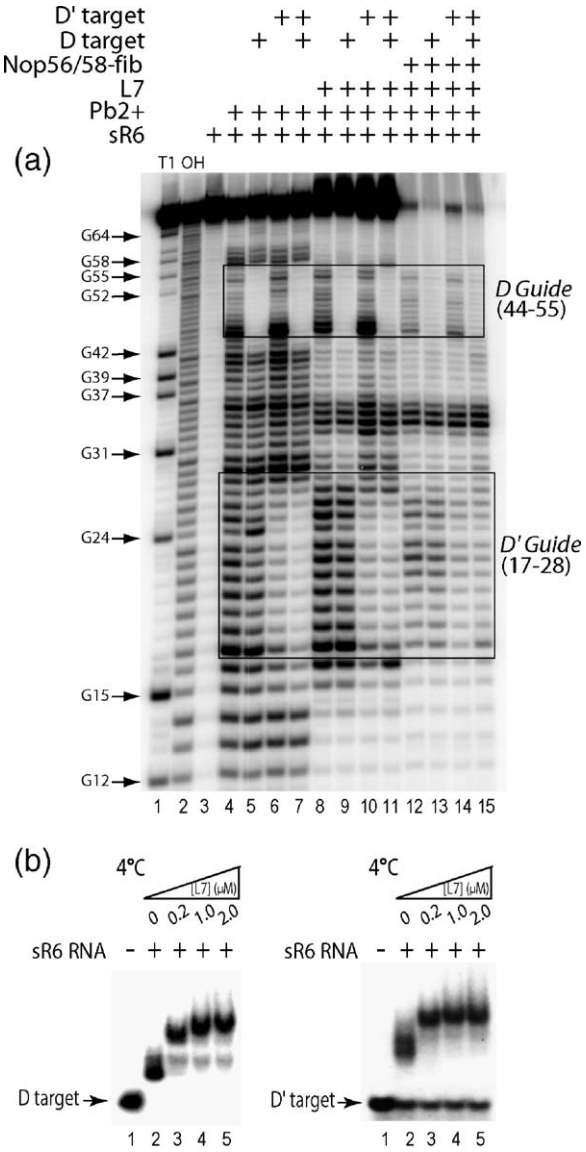

Figure 7. sR6 D and D′ guide regions are accessible throughout sRNP assembly. (a) Assessment of sR6 D and D′ guide region accessibility to target RNA oligonucleotide binding using Pb^{2+} cleavage probing. 5′-Radiolabeled sR6 was sequentially assembled with sRNP core proteins, incubated with D and/or D′ target RNAs, and then cleaved with Pb^{2+}. sRNA cleavage fragments were resolved on a denaturing polyacrylamide sequencing gel. Components of each assembly reaction are indicated above each gel lane. Nucleotide sequencing ladders were made by RNase T1 digestion (T1) and alkaline hydrolysis (OH). Box C, D, C′, and D′ sequences are enclosed by boxes and D and D′ guide sequences designated by brackets. (b) EMSA analysis of target RNA oligonucleotide binding to sR6 D and D′ guide sequences in the presence of L7 core protein. Radiolabeled D (left panel) and D′ (right panel) target RNA oligonucleotides were incubated with non-radiolabeled sR6 sRNA at 4 °C in the presence of increasing concentrations of L7. Free RNA, RNA–RNA hybrids, and assembled RNPs were resolved on native polyacrylamide gels at 4 °C.

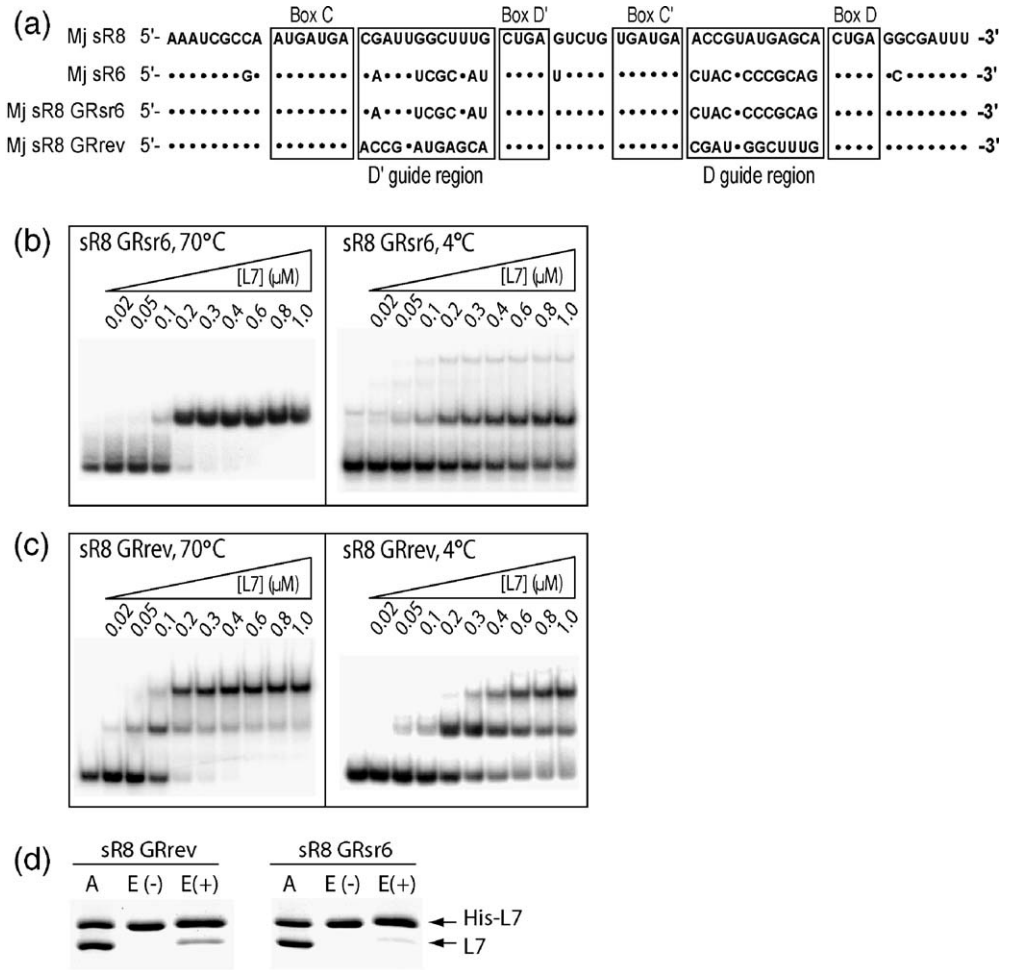

Figure 8. sRNA guide regions affect sRNA folding and L7 binding. (a) Primary sequence alignment of *M. jannaschii* sR8, sR6, sR8 GRsr6, and sR8 GRrev sRNAs. (b) and (c) sR8 GRsr6 and sR8 GRrev sRNAs bind one and two L7 core proteins, respectively, independent of temperature. Radiolabeled sRNA was incubated with increasing L7 concentrations at elevated and low temperatures and assembled RNPs resolved on polyacrylamide gels at 4 °C. (d) His-tag affinity purification of L7–sR8 GRsr6 and L7–sR8 GRrev complexes. His-tagged and non-tagged L7 proteins were incubated with indicated sRNAs at 70 °C and the assembled His-L7–sRNA complexes isolated by nickel affinity chromatography. Isolated proteins were resolved by SDS-PAGE and stained with Coomassie blue. A, His-tagged and non-tagged L7 proteins incubated with sRNAs; E(−), affinity purified L7 proteins incubated in the absence of added sRNA; E(+), affinity purified L7 proteins incubated in the presence of sRNA.

possess alternative guide sequences (Figure 8(a)). The first mutant switched the D and D′ guide regions within sR8 (sR8 GRrev), whereas the second mutant replaced D and D′ guide regions with the corresponding sR6 guide sequences (sR8 GRsr6). Initiation of sRNP assembly with L7 binding onto sR8 GRsr6 revealed L7 binding properties similar to that observed for sR6, with one L7 bound and only a weak second L7 interaction at both low and elevated temperatures (Figure 8(b) and (d)). As the major difference between sR6 and sR8 is their guide sequences, this result was anticipated and reinforced the idea that guide region sequence/structure influences initiation of sRNP assembly. Also anticipated was the binding of two L7 molecules to sR8 GRrev. However, the unexpected ability of sR8 GRrev to now bind L7 twice at low temperature, albeit less efficiently than at elevated temperature, indicated that individual guide regions/sequences can work in concert with flanking box C/D and C′/D′ motifs to influence overall sRNA structure and dynamics (Figure 8(c) and (d)). We have also analyzed the binding kinetics of L7 to sR8 GRrev and observed a hyperbolic binding curve at 4 °C consistent with one or two site binding but exhibiting no cooperativity. In contrast, L7 binding at 70 °C reveals sigmoidal binding and strong cooperativity with a Hill plot slope of nearly 2.0 (data not shown). These observations are consistent with the importance of sRNA remodeling for sRNP assembly and the influence of guide region sequence upon the remodeling pathway.

Analysis of full sRNP assembly for sR8 guide region mutants was carried out next using thermal denaturation analysis and temperature-dependent assembly. sR8 possessing sR6 or reversed sR8 D and D′ guide sequences exhibited the expected thermal stabilization of sRNA structure upon core protein

binding (Figure 9(a) and (b)). Notable, however, was the observation that reversing D and D′ guide regions had significant impact upon the melting profile of the free sR8 GRrev sRNA (Figure 9(b)). UV melt analysis revealed the replacement of sR8′s characteristic biphasic melting curve (Figure 2(b)) with a monophasic curve. This indicated that reversing the positioning of the D and D′ guide sequences significantly altered sRNA folded structure. Replacement of sR8 guide regions with the respective sR6 sequences resulted, as might be expected, in a monophasic curve that was characteristic of sR6 sRNA. Furthermore, replacement of sR6 guide regions with the corresponding sR8 guide sequences produced the expected biphasic melting curve (data not shown). Thus, individual guide sequences have the ability to fold the complete sRNA molecule into different conformations prior to core protein binding and sRNP assembly.

Core protein binding to the sR8 GRsr6 mutant demonstrated that substitution with sR6 guide sequences generated an sR8 molecule that exhibited the core protein binding characteristic of sR6 (Figure 9(c)). Interestingly, sR8 possessing switched D and D′ guide regions (sR8 GRrev) bound two L7 core proteins even at low temperature and required only elevated temperature for Nop56/58 binding (Figure 9(d)). Nuclease and Pb^{2+} probing of mutant sRNP assemblies has revealed unique cleavage patterns for these mutants distinct from either sR8 or sR6 during assembly, although the fully assembled complexes exhibited similar patterns (data not show). Assessment of the methylation capabilities of both mutants revealed activities similar to the wild-type sRNPs (Table 1). Together, these results support the idea that sRNA guide region sequences can fold into conformations which not only affect global sRNA structure, but also the initiation of sRNP assembly and the remodeling pathway followed to assemble functional sRNP complexes.

Discussion

Archaeal box C/D sRNP assembly requires elevated temperatures to enhance the dynamic nature of the sRNA and permit RNA remodeling essential for core protein binding. The binding of the core proteins then restricts flexibility as sRNA structure becomes more ordered. For box C/D

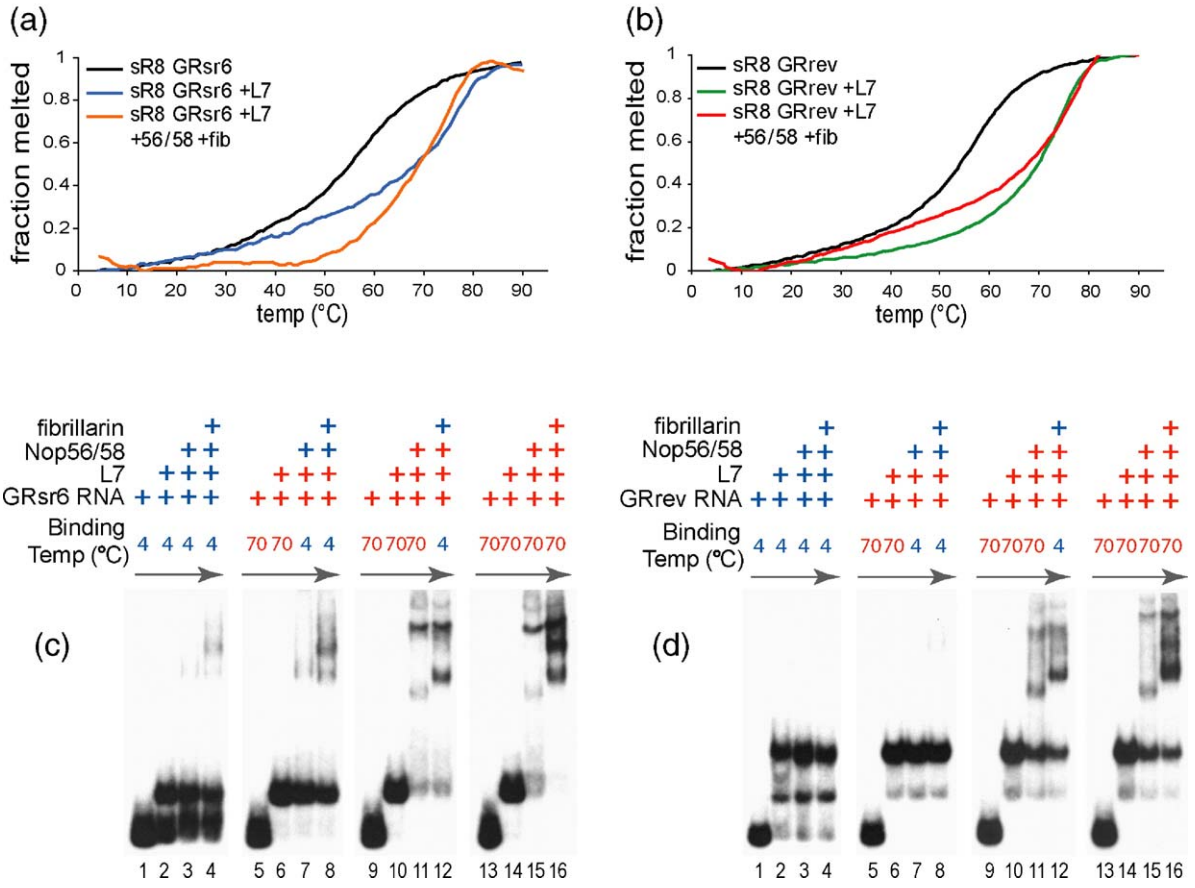

Figure 9. Altered sRNA guide regions affect sRNA structure and sRNP assembly. (a) and (b) Thermal denaturation analyses of sR8 GRsr6 and sR8 GRrev sRNP assembly. (c) and (d) Assembly of sR8 GRsr6 and sR8 GRrev sRNPs is temperature-dependent. Radiolabeled sRNAs were incubated sequentially with L7, Nop56/58, and fibrillarin core proteins at 4 °C or 70 °C. The resulting RNP complexes were resolved on native polyacrylamide gels at 4 °C. Indicated above each gel lane are the components for each assembly step with the respective incubation temperature. Arrows indicate the order of core protein addition for individual assembly reactions.

sRNAs, core protein binding at the box C/D and C′/D′ motifs stabilizes sRNA structure primarily through the establishment of K-turns. Bound core proteins may further provide a scaffold for the sRNA, exposing the guide sequences for target RNA base-pairing while establishing the necessary inter-RNP spacing required for nucleotide methylation. Comparison of different box C/D sRNAs has indicated that sRNP assembly can occur *via* different assembly pathways, both in terms of core protein binding and sRNA structural changes. Nevertheless, RNA structural remodeling upon core protein binding appears to be a common theme for each sRNA species in assembling an enzymatically active sRNA-guided nucleotide modification complex.

Box C/D sRNP assembly is initiated by L7 binding to the box C/D and/or C′/D′ motifs. The free and L7-bound K-turn fold of the box C/D motif has been well characterized by X-ray crystallography, computer simulations, and with FRET and biochemical analyses.[21,30,34,37–41,46–50] FRET analysis has revealed an inherent structural flexibility that becomes more ordered with increasing concentrations of Mg^{2+} and Na^{+}. Similarly, the binding of L7 stabilizes the K-turn motif, restricting its conformation and inducing a sharp kink in the RNA backbone. At both low and elevated temperatures, independent box C/D and C′/D′ K-turns bind L7 efficiently. However, when box C/D and C′/D′ motifs are juxtaposed in the same molecule, elevated temperature is critical for increasing the conformational dynamics of the sRNA to facilitate efficient L7 binding at both motifs. We have previously reported the cooperative nature of L7 binding to sR8 and the cross-talk interactions important for efficient methylation activities guided by both box C/D and C′/D′ RNPs.[30,36] Therefore, it is reasonable to suggest that formation of inter-RNP interactions critical for methylation activity may well be dependent upon the inherent structural flexibility of the sRNA itself.

Nop56/58 binding required prior L7 binding as well as elevated temperatures, indicating the importance of a defined K-turn structure and RNA structural flexibility for binding. The small changes in sRNA conformation upon Nop56/58 binding indicated that structural alterations, such as base stacking and nucleotide positioning, of the K-turns or adjacent guide regions are more subtle and specifically required for Nop56/58 binding. A crystal structure of this protein has suggested that the protein's extended coiled-coil domain may facilitate self-dimerization in the fully assembled sRNP, perhaps establishing inter-RNP interactions between the box C/D and C′/D′ complexes[42]. However, we have recently shown that this interaction is not required for sRNP assembly and is not likely to occur in the complete sRNP complex.[36] The observation that loss of the coiled-coil domain affects overall sRNP structure is, however, consistent with a structural role for Nop56/58 in establishing sRNA and sRNP conformations ultimately important for RNA-guided methylation.

In contrast to L7 and Nop56/58, fibrillarin does not require elevated temperature for binding and has only minor effects upon sRNA structure. The demonstrated dimerization of Nop56/58 and fibrillarin core proteins in solution is consistent with the idea that these two core proteins function in the sRNP as a dimer. We have previously proposed that Nop56/58 and fibrillarin form a protein scaffold or "platform".[36] It is upon this platform that the sRNA-target RNA duplex is formed and the base-paired target RNA for modification positioned. Recent work has suggested that in specific archaeal organisms, such as *Archaeoglobus fulgidus*, L7 may help position this platform on the target RNA *via* L7 protein–protein interactions with Nop56/58.[36] This core protein platform could establish an architectural bridge between both terminal and internal C/D motifs, providing inter-RNP spacing constraints necessary to position the fibrillarin active site for specific 2′-*O*-methylation of target RNA nucleotides according to the N+5 rule.[1,30,35] The need for sRNA structure to conform to this protein platform would also help explain the nature of Nop56/58 and fibrillarin-induced RNA remodeling.

The fibrillarin-Nop56/58 platform is anticipated to interact with D and D′ guide regions, ultimately positioning the methylase fibrillarin's catalytic domain at the target nucleotide. Protection of specific sR8 and sR6 guide region nucleotides upon Nop56/58 binding is consistent with this positioning, as observed in chemical/nuclease mapping experiments. However, equally notable is the enhanced digestion of specific guide nucleotides upon core protein binding demonstrating induced, and possibly distinct, structural changes in the guide regions. This is apparent in comparing sR8 and sR6 sRNP assemblies where guide regions of sR8 are not available for target RNA binding during sRNP assembly while those of sR6 are continuously exposed. Guide sequences vary with each specific sRNA species, and these differences in functional folding are clearly caused by the individual guide regions, as demonstrated by the sR8 mutant constructs possessing replaced or simply reversed guide sequences. Therefore, it is not surprising that individual sRNA species would exhibit distinct RNA remodeling pathways reflecting their unique guide sequences.

A model summarizing alternative folding and assembly pathways to a functional sRNP is presented in Figure 10. The guide sRNA is conformationally dynamic when free in solution. Transient formation of box C/D and/or C′/D′ K-turn structures allow L7 core proteins to bind and initiate sRNP assembly. Considering the diversity of guide sequences present in the various box C/D sRNAs, it is likely that numerous folding intermediates will be exhibited by the individual RNAs as they assemble RNP complexes. Unfavorable sRNA folding intermediates may become energetically trapped at these early assembly stages depending on the particular sRNA species, thereby generating alternative remodeling and assembly pathways. For example, L7

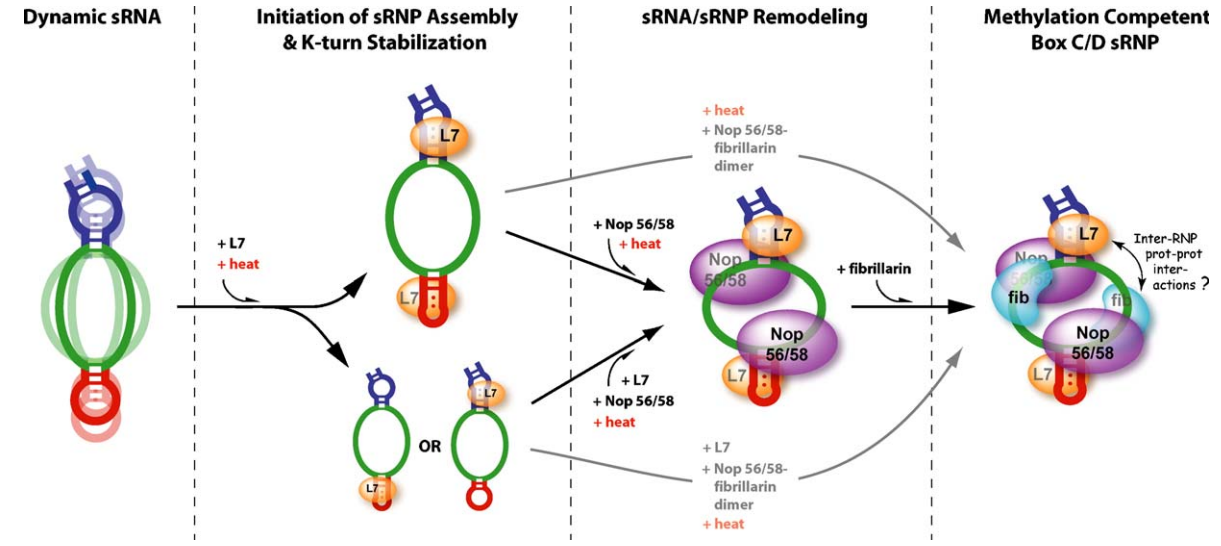

Figure 10. Archaeal box C/D sRNPs can follow different remodeling and assembly pathways.

may bind once or twice to one or both K-turn motifs. However, early assembly pathways begin to converge when Nop56/58 binds at elevated temperature, followed by addition of the methylase fibrillarin, which may either bind with or after Nop56/58. Binding of these core proteins further remodels the sRNA/sRNP structure to assemble complete box C/D and C′/D′ RNPs, expose the guide regions for target RNA binding, and establish the necessary inter-RNP spacing required for specific nucleotide methylation.

We have concluded that alternative sRNA folding schemes and sRNP assembly pathways may be followed by the many archaeal box C/D sRNAs. Thermophilic organisms such as *M. jannaschii* live at elevated growth temperatures.[51] Thus, the ambient environment could facilitate sRNA remodeling during the sRNP assembly process. However, for most organisms RNA helicases, such as DExH/D box family proteins, are likely to guide important RNA structural changes during RNP assembly. For example, the eukaryotic nucleolus possesses a large number of RNA helicases, underscoring their important roles in various steps of ribosome biogenesis. Two DExD/H box proteins in yeast, Prp43p and Dbp4p, were recently found to function in ribosome biogenesis and implicated in chaperoning snoRNA activity.[52–54] Box C/D snoRNP biogenesis in yeast requires Tip48 and Tip49 helicases whose presumed function is the rearrangement of RNA folded structures during RNP assembly.[25,55–57] Similarly, the human U3 snoRNA is associated with these same helicases during RNP biogenesis in the nucleoplasm.[57] RNA helicases are abundant in all kingdoms of life, suggesting that this class of proteins likely plays important structural roles in the biogenesis and function of numerous RNP complexes.

We have shown that archaeal box C/D sRNP assembly is dependent upon elevated temperature to facilitate the dynamic flexibility of sRNA structure necessary for core protein binding. This requirement for elevated temperature is reminiscent of *in vitro* assembly of *Escherichia coli* 30 S ribosomal subunits where heating steps during sequential ribosomal protein binding are necessary to facilitate assembly of a functional ribosome subunit.[58] However, protein-induced changes in RNA structure are not limited to elevated temperatures as recently demonstrated with the binding of SRP19 at ambient temperature to alter SRP RNA structure during RNP assembly.[59] Thus, remodeling of RNA structure facilitated by bound proteins appears to be a common and perhaps unifying theme in RNP assembly pathways. As with archaeal box C/D sRNPs, these RNA structural changes are also likely to be critical for RNP function.

Materials and Methods

RNA synthesis

Full length sR8, sR6, and the sR8 C/D and C′/D′ half-molecule RNAs were synthesized as described.[30] DNA oligonucleotides (Integrated DNA Technologies) were used for PCR-amplification of sR8 and sR8 sRNA genes. PCR amplification introduced a T7 promoter sequence at the 5′ end of the sRNA sequence and allowed introduction of sequence alterations in the sRNA coding region. sR8 (oligo 1), sR6 (oligo 4) sR8 GRrev (oligo 7), and sR8 GRsr6 (oligo 10) template DNA oligonucleotides were PCR-amplified with the following DNA primer pairs: sR8 (primers 2 and 3), sR6 (primers 5 and 6), sR8 GRrev (primers 8 and 9) and sR8 GRsr6 (11 and 12). The sequence of all templates and PCR primers are presented below (5′ to 3′).

(1)AAATCGCGAATGATGACAATTTCGCTATCTGATTCTGTGATGACTACTCCCGCAGCTGAGCCGATTT

(2)AAATCGCCAATGATGAACCGTATGAGCACTGAGTCTGTGATGACGATTGGCTTTGCTGAGGCGATTT

(3)AAATCGCCAATGATGACAATTTCGCTATCTGAGTCTGTGATGACTACTCCCGCAGCTGAGGCGATTT

(4)CTAATACGACTCACTATAGGCCAAACTGGC-GATGATGACAATTT
(5)AAACTGGCTCAGCTGCGGGAGTA.
(6)CTAATACGACTCACTATAGGCCAAATCGCCAAT-GATGAACCGTATGAGCA
(7)AAATCGCCTCAGCAAAGCCAATCG.
(8)CTAATACGACTCACTATAGGCCAAATCGCCAAT-GATGACAATTTCGCTAT
(9)AAATCGCCTCAGCTGCGGGAGTAG

sRNAs were *in vitro* transcribed using Ampliscribe Flash T7 Transcription Kits (Epicentre) and gel-purified by denaturing polyacrylamide gel electrophoresis (PAGE). Purified RNAs were radiolabeled at the 5′ terminus by first digesting with calf intestine alkaline phosphatase (CIAP; Promega) then radiolabeling using T4 polynucleotide kinase (PNK, Promega) and [γ-^{32}P]ATP (MP Biomedicals). Radiolabeled sRNAs were re-purified using spin columns (Sephadex G-25 resin) or by denaturing PAGE. Target RNA oligonucleotides were chemically synthesized by Dharmacon RNA Technologies, Inc. or Integrated DNA Technologies. Target RNA sequences are listed below (5′ to 3′). Nucleotides methylated at the 2′-*O* position are designated with an m preceding the nucleotide. sR8 D target: AUGCUCAUACGGUC; sR8 D-CH_3 target: UGAUGCU-mCAUACGGUCUGCU; sR8 D′ target: GCUCAAAGC-CAAUCGC; sR8 D′-CH_3 target: GCUCAAAmGC-CAAUCGC; sR6 D target: ACUGCGGGAGUAGC; sR6 D-CH_3 target: ACUGCmGGGAGUAG C; sR6 D′ target: GCUAUAGCGAAAUUGC; sR6 D′-CH_3 target: GCUAUAGmCGAAAUUGC.

Electrophoretic analysis of RNP assembly

M. jannaschii box C/D sRNP core proteins L7, Nop56/58, and fibrillarin were expressed in *E. coli* and purified as described.[30] For electrophoretic mobility-shift analysis (EMSA) of L7 binding to sRNAs, 5′-radiolabeled (0.2 pmol and 1×10^4 cpm) sRNA was incubated with increasing concentrations of L7 protein in binding buffer (20 mM Hepes (pH 7.0), 150 mM NaCl, 1.5 mM $MgCl_2$, 10% (w/v) glycerol) supplemented with 0.5 mg/ml of tRNA (final volume of 20 μl). Reactions were incubated at 70 °C for 10 min and then cooled to 23 °C. Higher-order RNP assembly contained 20 pmol of L7, 32 pmol of Nop56/58, and 32 pmol of fibrillarin and a final concentration of 1.5 mg/ml tRNA. Complexes were resolved on native 4% (w/v) or 6% polyacrylamide gels buffered with 25 mM potassium phosphate (pH 7.0), and 2% glycerol. Gels were vacuum-dried and visualized using a phosphorimager or by autoradiography. For temperature-dependent analysis of RNP assembly, reactions were either assembled on ice or heated to 70 °C, then equilibrated on ice before resolving on native polyacrylamide gels at 4 °C. Radiolabeled target RNA and L7 binding to sRNAs at 4 °C was carried out by binding target RNA to the guide sRNA, then cooling and incubating on ice for 15 min with increasing concentrations of L7. Assembled complexes were resolved on native polyacrylamide gels at 4 °C.

Nuclease and Pb^{2+} mapping of sRNA and sRNP

Radiolabeled sRNA ($\geq1\times10^5$ cpm) was incubated with 20 pmol of L7, 32 pmol of Nop56/58, 32 pmol of fibrillarin, and/or 20 of pmol of target RNA(s) in assembly buffer (20 mM Hepes (pH 7.0), 100 mM NaCl, 3 mM $MgCl_2$, 0.2 mM EDTA) containing 0.5 mg/ml of tRNA. Reactions were incubated at 70 °C then at 50 °C before cooling to 23 °C. Mung bean nuclease (Epicentre) was added to a final of 0.63 units/μl and reactions incubated at 23 °C for 8–10 min. Alternatively, lead acetate was added to a final concentration of 2 mM. For mapping of low temperature L7 binding, protein–RNA complexes were assembled at either 70 °C or on ice and then probed with mung bean nuclease on ice. T1 digestion ladders were generated by incubating 5′-radiolabeled sRNA with 0.3 mg/ml of tRNA and 0.05 unit/μl of RNase T1 (Ambion) in assembly buffer at 23 °C. Alkaline hydrolysis ladders were generated by incubating 5′-radiolabeled sRNA with 0.3 mg/ml of tRNA in 10 mM $NaHCO_3$ (pH 10.0), 1 mM EDTA at 95 °C. No reaction (NR) samples were handled identically except without added nuclease or Pb^{2+}. All reactions were stopped by addition of ten volumes of 2% (w/v) $LiClO_4$ in acetone. Pellets were collected by centrifugation, washed with acetone, and then air-dried. RNA samples were resuspended in loading buffer (1× Tris-borate-EDTA, 4 M urea, 0.25 mg/ml bromophenol blue, 0.25 mg/ml xylene cyanol, 12% (w/v) sucrose), boiled for 5 min, and resolved on 14% polyacrylamide sequencing gels containing Tris-borate-EDTA buffer (pH 8.3), and 7 M urea. Vacuum-dried gels were visualized using a phosphorimager.

Circular dichroism spectroscopy

Circular dichroism spectroscopic analysis was carried out using a Jasco model J-600 spectropolarimeter with a water-cooled 1 cm cuvette. Each experiment consisted of a minimum of five wavelength scans from 300 nm −220 nm in 1 nm steps. Data presented are the average of three or more separate experiments. For L7 binding to sR8, sR8 (1 μM) was incubated with and without L7 (2 μM) in buffer C (20 mM cacodylate (pH 7.0), 100 mM NaCl, 1 mM $MgCl_2$) at 4 °C or 70 °C then equilibrated to 4 °C before analysis. For CD analysis of higher-order sRNP assembly, L7, Nop56/58, and fibrillarin proteins at final concentrations of 2 μM each were incubated at 70 °C under different combinations with and without sRNA (1 μM) in buffer C then analyzed at 23 °C. All presented CD spectra are subtracted for buffer and protein spectra contributions in the 220 nm −300 nm range. CD spectra of free sRNA in solution when previously incubated at either high or low temperature were identical, except for a small loss of total signal (~2%) due to RNA degradation from sample heating and cooling that was observed and accounted for in control experiments.

Thermal denaturation analysis

Thermal denaturation analysis of sRNAs and sRNPs was carried out using a CARY Varian model 3 UV-Vis spectrophotometer. Absorbance was monitored at 260 nm in a 1 cm quartz cuvette. sRNA (0.83 μM) in buffer UV (20 mM potassium phosphate (pH 7.0), 100 mM NaCl, 1 mM $MgCl_2$) was annealed and denatured twice from 4 °C to 95 °C at a ramp rate of 2 °C/min and absorbance collected at a rate of one reading per 0.5 °C. Values were averaged, normalized and plotted as a function of temperature. Analysis of thermal stabilization by full sRNP assembly used 2 μM of L7, Nop56/58, and fibrillarin in combinations incubated with or without sR8. Protein and buffer contributions to UV absorbance were subtracted from the absorbance data before normalization and plotting.

Affinity isolation of assembled L7–sRNA complexes

L7 occupancy on the sRNA box C/D and C′/D′ motifs was evaluated by affinity chromatography. N-terminally His(6X)-tagged L7 was incubated with untagged L7 (fivefold molar excess) in the presence or absence of sRNA (fivefold molar excess) in buffer B (10 mM Hepes (pH 7.0), 150 mM NaCl, 1.5 mM $MgCl_2$, 10% (w/v) glycerol, 0.5 mg/ml tRNA) at 70 °C for 10 min. Reactions were cooled to 23 °C, passed over Ni-NTA His-bind resin (Novagen), and the resin washed with buffer E (10 mM Hepes (pH 7.0), 150 mM NaCl, 1.5 mM $MgCl_2$, 10% glycerol, 50 mM imidazole, 0.007% (w/v) SDS, 0.1% (v/v) Triton X-100). Bound L7-sRNA complexes were eluted in buffer B containing 500 mM imidazole. Eluted proteins were acetone precipitated, resuspended in SDS loading buffer, and resolved on 16% SDS–polyacrylamide gels. Resolved proteins were visualized by Coomassie brilliant blue G-250 staining.

In vitro methylation assays

In vitro 2′-*O*-methylation assays for assembled box C/D sRNPs were carried out as described.[30] Aliquots in triplicate were taken at 0 and 60 min time points, trichloroacetic acid-precipitated, washed, and incorporation of $[^3H]CH_3$ into D or D′ target RNAs determined by scintillation counting. Incorporation of $[^3H]CH_3$ into target RNAs previously methylated at the target nucleotide served as controls and were subtracted from experimental levels.

Acknowledgements

We thank the Paul Wollenzien and Kevin Weeks laboratories for their advice on nuclease and Pb^{2+} mapping techniques and Bernard Brown for critical reading of the manuscript. This work was supported by NSF grant MCB 0543741 (to E.S.M.) and NIH grant 2R01-GM23037 (to P.F.A.).

References

1. Kiss-Laszlo, Z., Henry, Y., Bachellerie, M., Caizergues-Ferrer, M. & Kiss, T. (1996). Site-specific ribose methylation of preribosomal RNA: a novel function for small nucleolar RNAs. *Cell*, **85**, 1077–1088.
2. Nicoloso, M., Qu, L. H., Michot, B. & Bachellerie, J. P. (1996). Intron-encoded, anti-sense small nucleolar RNAs: the characterization of nine novel species points to their direct role as guides for the 2′-*O*-ribose methylation of rRNAs. *J. Mol. Biol.* **260**, 178–195.
3. Tollervey, D. (1996). Small nucleolar RNAs guide ribosomal RNA methylation. *Science*, **273**, 1056–1057.
4. Dennis, P. P., Omer, A. & Lowe, T. (2001). A guided tour: small RNA function in Archaea. *Mol. Microbiol.* **40**(3), 509–519.
5. Bachellerie, J. P., Cavaille, J. & Huttenhofer, A. (2002). The expanding snoRNA world. *Biochimie*, **84**, 775–790.
6. Terns, M. & Terns, R. (2002). Small nucleolar RNAs: versatile trans-acting molecules of ancient evolutionary origin. *Gene Expr.* **10**, 17–39.
7. Omer, A., Ziesche, S., Decatur, W., Fournier, M. J. & Dennis, P. (2003). RNA-modifying machines in Archaea. *Mol. Microbiol.* **48**, 617–629.
8. Decatur, W. A. & Fournier, M. J. (2003). RNA-guided nucleotide modification of ribosomal and other RNAs. *J. Biol. Chem.* **278**, 695–698.
9. Balakin, A. G., Smith, L. & Fournier, M. J. (1996). The RNA world of the nucleolus: two major families of small RNAs defined by different box elements with related functions. *Cell*, **86**, 823–834.
10. Kiss-Laszlo, Z., Henry, Y. & Kiss, T. (1998). Sequence and structural elements of methylation guide snoRNAs essential for site-specific ribose methylation of pre-rRNA. *EMBO J.* **17**, 797–807.
11. Vidovic, I., Nottrot, S., Hartmuth, K., Luhrmann, R. & Ficner, R. (2000). Crystal structure of the spliceosomal 15.5 kDa protein bound to a U4 snRNA fragment. *Mol. Cell*, **6**, 1331–1342.
12. Watkins, N. J., Segault, V., Charpertier, B., Nottrott, S., Fabrizio, P., Bachi, A. *et al.* (2000). A common core RNP structure shared between the small nucleolar box C/D RNPs and the spliceosomal U4 snRNP. *Cell*, **103**, 457–466.
13. Gaspin, C., Cavaille, J., Erauso, G. & Bachellerie, J. P. (2000). Archaeal homologs of eukaryotic methylation guide small nucleolar RNAs: lessons from the *Pyrococcus* genomes. *J. Mol. Biol.* **297**, 895–906.
14. Omer, A. D., Lowe, T. M., Russell, A. G., Ebhardt, H., Eddy, S. R. & Dennis, P. P. (2000). Homologs of small nucleolar RNAs in Archaea. *Science*, **288**, 517–522.
15. Dennis, P. P. & Omer, A. (2005). Small non-coding RNAs in Archaea. *Current Opin. Microbiol.* **8**, 685–694.
16. Cavaille, J., Nicoloso, M. & Bachellerie, J. P. (1996). Targeted ribose methylation of RNA in vivo directed by tailored antisense RNA guides. *Nature*, **383**, 732–735.
17. Caffarelli, E., Fatica, A., Prislei, S., DeGregorio, E., Fragapane, P. & Bozzoni, I. (1996). Processing of the intron-encoded U16 and U18 snoRNAs: the conserved C and D boxes control both the processing reaction and the stability of the mature snoRNA. *EMBO J.* **15**, 1121–1131.
18. Watkins, N., Leverette, R., Xia, L., Andrews, M. & Maxwell, E. S. (1996). Elements essential for processing intronic U14 snoRNA are located at the termini of the mature snoRNA sequence and include conserved nucleotide boxes C and D. *RNA*, **2**, 118–133.
19. Wang, H., Boisvert, D., Kim, K., Kim, R. & Kim, S. H. (2000). Crystal structure of a fibrillarin homologue from *Methanococcus jannaschii*, a hyperthermophile, at 1.6 Å resolution. *EMBO J.* **19**, 317–323.
20. Galardi, S., Fatica, A., Bachi, A., Scaloni, A., Presutti, C. & Bozzoni, I. (2002). Purified box C/D snoRNPs are able to reproduce site-specific 2′-*O*-methylation of target RNA in vitro. *Mol. Cell. Biol.* **22**, 6663–6668.
21. Kuhn, J., Tran, E. & Maxwel, E. S. (2002). Archaeal ribosomal protein L7 is a functional homolog of the eukaryotic 15.5 kD/Snu13p snoRNP core protein. *Nucl. Acids Res.* **30**, 931–941.
22. Gautier, T., Berges, T., Tollervey, D. & Hurt, E. (1997). Nucleolar KKE/D repeat proteins Nop56p and Nop58p interact with Nop1p and are required for ribosome biogenesis. *Mol. Cell. Biol.* **17**, 7088–7098.
23. Lafontaine, D. L. & Tollervey, D. (1999). Nop58p is a common component of the box C+D snoRNPs that is required for snoRNA stability. *RNA*, **5**, 455–467.
24. Lafontaine, D. L. & Tollervey, D. (2000). Synthesis and assembly of the box C+D small nucleolar RNPs. *Mol. Cell. Biol.* **20**, 2650–2659.

25. Newman, D., Kuhn, J., Shanab, G. & Maxwell, E. S. (2000). Box C/D snoRNA-associated proteins: two pairs of evolutionarily ancient proteins and possible links to replication and transcription. *RNA*, **6**, 861–879.
26. Cahill, N., Friend, K., Speckman, W., Li, Z., Terns, R., Terns, M. & Steitz, J. A. (2002). Site-specific cross-linking analyses reveal an asymmetric distribution for a box C/D snoRNP. *EMBO J.* **21**, 3816–3828.
27. Szewczak, L. W., DeGregorio, S., Strobel, S. & Steitz, J. A. (2002). Exclusive interaction of the 15.5 kD protein with the terminal box C/D motif of a methylation guide snoRNP. *Chem. Biol.* **9**, 1095–1107.
28. d'Orval, B., Bortolin, M., Gaspin, C. & Bachellerie, J. P. (2001). Box C/D RNA guides for the ribose methylation of archaeal tRNAs: the $tRNA^{Trp}$ intron guides the formation of two ribose-methylated nucleosides in the mature $tRNA^{Trp}$. *Nucl. Acids Res.* **29**, 4518–4529.
29. Omer, A., Ziesche, S., Ebhardt, H. & Dennis, P. (2002). In vitro reconstitution and activity of a C/D box methylation guide ribonucleoprotein complex. *Proc. Natl Acad. Sci. USA*, **99**, 5289–5294.
30. Tran, E. J., Zhang, X. & Maxwell, E. S. (2003). Efficient RNA 2′-*O*-methylation requires juxtaposed and symmetrically assembled archaeal box C/D and C′/D′ RNPs. *EMBO J.* **22**, 3930–3940.
31. Rashid, R., Aittaleb, M., Chen, Q., Spiegel, K., Demeler, B. & Li, H. (2003). Functional requirement for symmetric assembly of archaeal box C/D small ribonucleoprotein particles. *J. Mol. Biol.* **333**, 295–306.
32. Bortolin, M.-L., Bachellerie, J. P. & Clouet-d'Orval, B. (2003). *In vitro* RNP assembly and methylation guide activity of an unusual box C/D RNA, *cis*-acting archaeal pre-$tRNA^{Trp}$. *Nucl. Acids Res.* **31**, 6524–6535.
33. Singh, S. K., Gurha, P., Tran, E. J., Maxwell, E. S. & Gupta, R. (2004). Sequential 2′-*O*-methylation of Archaeal pre-$tRNA^{Trp}$ nucleotides is guided by the intron-encoded but trans-acting box C/D ribonucleoprotein of pre-tRNA. *J. Biol. Chem.* **279**, 47661–47671.
34. Rozhdestvensky, T. S., Tang, T. H., Tchirkova, I. V., Brosius, J., Bachellerie, J. P. & Huttenhofer, A. (2003). Binding of L7Ae protein to the K-turn of archaeal snoRNAs: a shared RNA binding motif for C/D and H/ACA box snoRNAs in Archaea. *Nucl. Acids Res.* **31**, 869–877.
35. Tran, E. J., Zhang, X., Lackey, L. & Maxwell, E. S. (2005). Conserved spacing between the box C/D and C′/D′ RNPs of the archaeal box C/D sRNP complex is required for efficient 2′-*O*-methylation of target RNAs. *RNA*, **11**, 285–293.
36. Zhang, X., Champion, E. A., Tran, E., Brown II, B. A., Baserga, S. J. & Maxwell, E. S. (2006). The coiled-coil domain of the Nop56/58 core protein is dispensable for sRNP assembly but is critical for archaeal box C/D sRNP-guided nucleotide methylation. *RNA*, **12**, 1092–1103.
37. Klein, D. J., Schmeing, T. M., Moore, P. B. & Steitz, T. A. (2001). The kink-turn: a new RNA secondary structure motif. *EMBO J.* **20**, 4214–4221.
38. Moore, T., Zhang, Y., Fenley, M. O. & Li, H. (2004). Molecular basis of box C/D RNA-protein interactions: cocrystal structure of archaeal L7Ae and a box C/D RNA. *Structure*, **12**, 807–818.
39. Hama, T. & Ferre-D'Amare, A. R. (2004). Structure of protein L7Ae bound to a k-turn derived from an archaeal box H/ACA sRNA at 1.8 Å resolution. *Structure*, **12**, 893–903.
40. Suryadi, J., Tran, E. J., Maxwell, E. S. & Brown, B. A., II (2005). The crystal structure of *Methanocaldococcus jannaschii* multifunctional L7Ae RNA-binding protein reveals an induced-fit interaction with the box C/D RNAs. *Biochemistry*, **44**, 9657–9672.
41. Turner, B., Melcher, S. A., Wilson, T. J., Norman, D. G. & Lilley, D. M. J. (2005). Induced fit of RNA on binding the L7Ae protein to the kink-turn motif. *RNA*, **11**, 1192–1200.
42. Aittaleb, M., Rashid, R., Chen, Q., Palmer, J., Daniels, C. & Li, H. (2003). Structure and function of Archaeal box C/D sRNP core proteins. *Nature Struct. Biol.* **10**, 256–263.
43. Fasman, G. D. (1996). In *Circular Dichroism and the Conformational Analysis of Biomolecules* p. 738, Springer Press, New York, N.Y.
44. Pan, T. & Sosnick, T. R. (1997). Intermediates and kinetic traps in the folding of a large ribozyme revealed by circular dichroism and UV absorbance spectroscopies and catalytic activity. *Nature Struct. Biol.* **4**, 931–938.
45. Manival, X., Ghisolfi-Nieto, L., Joseph, G., Bouvet, P. & Monique, E. (2001). RNA-binding strategies common to cold-shock domain- and RNA recognition motif-containing proteins. *Nucl. Acids Res.* **29**, 2223–2233.
46. Goody, T., Melcher, S. E., Norman, D. G. & Lilley, D. M. J. (2004). The kink-turn motif in RNA is dimorphic, and metal ion-dependent. *RNA*, **10**, 254–264.
47. Matsumura, S., Ikawa, Y. & Inoue, T. (2003). Biochemical characterization of the kink-turn RNA motif. *Nucl. Acids Res.* **31**, 5544–5551.
48. Cojocaru, V., Klement, R. & Jovin, T. M. (2005). Loss of G-A base pairs is insufficient for achieving a large opening of U4 snRNA k-turn motif. *Nucl. Acids Res.* **33**, 3435–3446.
49. Wozniak, A. K., Nottrott, S., Kuhn-Holsken, E., Schroder, G. F., Grubmuller, H., Luhrmann, R., Seidel, C. A. M. & Oesterhelt, F. (2005). Detecting protein-induced folding of the U4 snRNA kink-turn by single-molecule multiparameter FRET measurements. *RNA*, **11**, 1545–1554.
50. Szewczak, L. B., Gabrielsen, J. S., DeGregorio, S. J., Strobel, S. A. & Steitz, J. A. (2005). Molecular basis for RNA kink-turn recognition by the h15.5K small RNP protein. *RNA*, **11**, 1407–1419.
51. Haney, P. J., Badger, J. H., Buldak, G. L., Reich, C. I., Woese, C. R. & Olsen, G. J. (1999). Thermal adaptation analyzed by comparison of protein sequences from mesophilic and extremely thermophilic *Methanococcus* species. *Proc. Natl Acad. Sci. USA*, **96**, 3578–3583.
52. Leeds, N. B., Small, E. C., Hiley, S. L., Hughes, T. R. & Staley, J. P. (2006). The splicing factor Prp43p, a DEAH box ATPase, functions in ribosome biogenesis. *Mol. Cell. Biol.* **26**, 513–522.
53. Combs, D. J., Nagel, R. J., Ares, M., Jr. & Stevens, S. W. (2006). Prp43p is a DEAH-box spliceosome disassembly factor essential for ribosome biogenesis. *Mol. Cell. Biol.* **26**, 523–534.
54. Kos, M. & Tollervey, D. (2005). The putative RNA helicase Dbp4p is required for release of the U14 snoRNA from preribosomes in *Saccharomyces cerevisiae*. *Mol. Cell*, **20**, 53–64.
55. King, T. H., Decatur, W. A., Bertrand, E., Maxwell, E. S. & Fournier, M. J. (2001). A well-connected and conserved nucleoplasmic helicase is required for production of box C/D and H/ACA snoRNAs and Localization of snoRNP proteins. *Mol. Cell. Biol.* **21**, 7731–7746.
56. Watkins, N. J., Dickmanns, A. & Luhrmann, R. (2002). Conserved stem II of the box C/D motif is essential for

nucleolar localization and is required, along with the 15.5 K protein, for the hierarchical assembly of the box C/D snoRNP. *Mol. Cell. Biol.* **22**, 8342–8352.
57. Watkins, N. J., Lemm, I., Ingelfinger, D., Schneider, C., Hobbach, M., Urlaub, H. & Luhrmann, R. (2004). Assembly and maturation of the U3 snoRNP in the nucleoplasm in a large dynamic multiprotein complex. *Mol. Cell*, **16**, 789–798.
58. Culver, G. M. & Noller, H. F. (1999). Efficient reconstitution of functional *Escherichia coli* 30S ribosomal subunits from a complete set of recombinant small subunit ribosomal proteins. *RNA*, **5**, 832–843.
59. Hainzl, T., Huang, S. & Sauer-Eriksson, A. E. (2005). Structural insights into SRP RNA: An induced fit mechanism for SRP assembly. *RNA*, **11**, 1043–1050.

Edited by J. Doudna

(Received 12 May 2006; received in revised form 21 July 2006; accepted 29 July 2006)
Available online 4 August 2006